

Controllable Preparation of V₂O₅ Hollow Microspheres as Cathode Materials for Lithium-Ion Batteries

Xinxin An^{1, §}, Qiong Su^{2, §}, Yanglin Liu¹, Anqiang Pan^{1,*}

¹ School of Materials Science and Engineering, Central South University, Changsha 410083, PR China.

² Hunan Yingzi Biotechnology Incorporation, Changsha, 410083, Hunan, PR China

§ the authors are contributed equally to this work

*E-mail: pananqiang@csu.edu.cn

Received: 13 April 2017 / Accepted: 11 May 2017 / Published: 12 June 2017

Hollow-structured vanadium oxides with tunable interiors have attracted significant attention in energy storage and conversion systems. In this work, we report the continuous structural engineering of VO₂ solid microspheres utilizing a second solvothermal solution under the driving force of an Ostwald-ripening mechanism. The VO₂ microspheres with diversified interior structures, such as yolk-shelled, double-shelled and complete hollow microspheres, were obtained by simply controlling the solvothermal duration in the new solvothermal solution. The obtained VO₂ microspheres were converted into V₂O₅ microspheres with good structural preservation after calcination. As a cathode material for lithium batteries, the V₂O₅ hollow microspheres exhibited high capability and good cycling stability. A high specific discharge capacity of 129.4 mA h g⁻¹ was obtained for the V₂O₅ hollow microsphere electrode, which retained 114.5 mA h g⁻¹ after 200 cycles. The superior electrochemical properties were attributed to the promising features of the hollow microspheres.

Keywords: Vanadium oxide; hollow microspheres; solvothermal synthesis; lithium batteries

1. INTRODUCTION

Because of their high energy density, environmental friendliness, long lifespan, and design flexibility[1-3], rechargeable lithium-ion batteries (LIBs) are widely used in current portable electronic devices, such as electric vehicles (EVs) and hybrid electric vehicles (HEVs)[4-7]. The performances of LIBs largely depend on their electrode materials [8, 9]. Therefore, developing advanced electrode materials with high performances is urgently needed to meet the aggressive demands of portable electronic devices and high-power electric vehicles [1, 10].

Vanadium pentoxide (V_2O_5), a desirable alternative cathode material, has drawn much attention due to its low cost, abundant resources, high output voltage[11, 12] and high theoretical capacity (294 mA h g^{-1} for two lithium ions per formula)[13-16]. Nevertheless, the practical use of V_2O_5 has been held back due to the low ionic diffusivity of Li^+ ions (10^{-13} to 10^{-12} $cm^2 S^{-1}$), moderate electrical conductivity (10^{-3} to 10^{-2} cm^{-1}) and poor structural stability[5, 17-20]. Recently, porous- or hollow-structured V_2O_5 electrode materials have exhibited promising Li^+ ion storage properties owing to their improved electrolyte penetration, easy accommodation of volumetric changes upon Li^+ intercalation/deintercalation, and lower polarization[21]. Moreover, hollow microspheres can alleviate the aggregation of the electrode materials during repeated cycles. To date, various strategies, such as hard-templating methods[22], solvothermal treatments[23, 24] and self-templating approaches[25, 26], have been reported for the fabrication of hollow-structured V_2O_5 microspheres, which exhibit improved electrochemical performances. Pan et al. reported the preparation of VO_2 microspheres with diversified interior structures by a time-dependent Ostwald-ripening process.[25] However, the entire process was studied in a single solvent. It would be interesting to study the structural evolution of the obtained VO_2 microspheres in another solvothermal solvent, which would expand the feasibility of fabricating hollow-structured V_2O_5 microspheres with diversified interior structures.

In this paper, we report the controllable synthesis of VO_2 hollow microspheres with yolk-shell, double-shell and single-shell interior structures by a second solvothermal process using the solvothermally prepared VO_2 solid microspheres as starting materials. The VO_2 microspheres are robust and can be readily converted into V_2O_5 hollow microspheres with good structural preservation by calcination in air. As cathode materials for LIBs, the obtained V_2O_5 hollow microspheres manifest high specific capacity and superior cycling stability.

2. EXPERIMENTAL

2.1 Preparation of materials

VO_2 solid microspheres: All the chemicals and solvents were of analytical grade and used without further purification. VO_2 solid microspheres were solvothermally fabricated according to a previous report[25]. In a typical synthesis, V_2O_5 (1.2 g) and oxalic acid in a stoichiometric ratio of 1:3 were added into 40 mL of distilled water and magnetically stirred at 60 °C for several hours to get a clear, blue solution of VOC_2O_4 . The obtained VOC_2O_4 solution (3 mL) and 30 mL isopropanol were added into a 50 mL PPL container and magnetically stirred at room temperature for 20 min. Then, the container was sealed in a stainless-steel autoclave and treated at 200 °C for 2 h. After cooling to room temperature naturally, the precipitates were collected by a centrifuge and washed with absolute alcohol three times. The VO_2 solid microspheres were obtained by drying at 80 °C for 12 h.

V_2O_5 hollow microspheres: The as-prepared VO_2 solid microspheres were homogeneously dispersed in 30 mL of an ethylene glycol (EG) solution, and the obtained mixture was sealed in a 50-mL PPL-lined stainless-steel autoclave at 210 °C for 12, 24 or 36 h. After cooling naturally, black precipitates were collected and washed with absolute alcohol three times before drying at 80 °C for 12

h. The obtained samples were designated as VO₂-12 h, VO₂-24 h and VO₂-36 h. After annealing at 350 °C for 2 h with a heating rate of 1 °C min⁻¹, the obtained solvothermal products were converted into V₂O₅ hollow microspheres.

2.2 Structural characterization

The crystalline structures of all the products were determined by X-ray diffraction (XRD, Rigaku D/max 2500 XRD with Cu K α radiation, $\lambda=1.54178$ Å). The morphologies and structures of the synthesized products were determined by scanning electron microscopy (SEM, FEI Nova NanoSEM 230) and transmission electron microscopy (TEM, JEOL JEM-2100F).

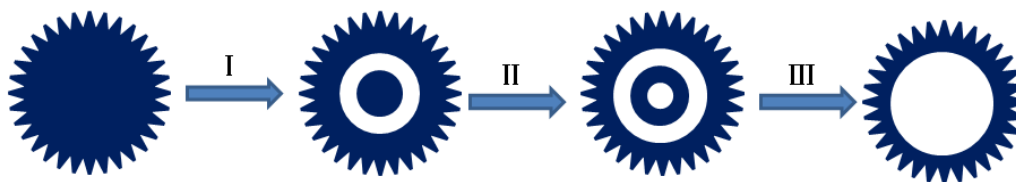
2.3 Electrochemical measurements

The electrochemical properties of the V₂O₅ hollow microspheres were investigated in two-electrode coin-type cells (CR 2016). V₂O₅, acetylene black, and polyvinylidene fluoride (PVDF) binder in a weight ratio of 70:20:10 were mixed and then dispersed in an N-methyl-2-pyrrolidone (NMP) solution to make a slurry, which was coated on aluminum foil and dried in a vacuum oven at 100 °C overnight prior to coin cell assembly. The half-cells were assembled in a glove box (MBraun, Germany) filled with ultrahigh-purity argon. A polypropylene membrane was used as the separator, and 1 M LiPF₆ dissolved in ethylene carbonate/dimethyl carbonate (EC/DMC) = 1:1 (volume ratio) was used as the electrolyte. Lithium metal was employed as the counter and reference electrodes. Cyclic voltammetry (CV; 2.5–4.0 V, 0.1 mV s⁻¹) measurements were performed by a CHI 660C electrochemical workstation. The galvanostatic charge-discharge characteristics of the cells were obtained on a Land Battery Tester (Land CT 2001A, Wuhan, China) in the voltage range of 2.5-4.0 V (versus Li/Li⁺) at room temperature. The mass loading of the cathode material was approximately 1.5 mg cm⁻², and the specific capacity was calculated based on the weight of the active material only.

3. RESULTS AND DISCUSSION

3.1 Morphology and structure

Scheme 1 illustrates the formation of the hollow microspheres with diversified interior structures from the solid VO₂ microspheres, which were solvothermally prepared in an isopropanol solution according to our previous report[25]. The structural evolution from the solid microspheres to the yolk-shelled, double-shelled and complete hollow-structured microspheres occurred in the second solvothermal treatment in ethylene glycol (EG) and are dependent on the solvothermal duration. Under the driving force of Ostwald-ripening, the solid microspheres were first converted into the yolk-shell structure (I, 12 h), then to the double-shelled VO₂ microspheres (II, 24 h), and finally to the total hollow-structured VO₂ microspheres at an extended solvothermal time (III, 36 h).



Scheme 1. Illustration of the formation of VO₂ hollow microspheres in EG solvent with different solvothermal times: 12 h (I), 24 h (II), and 36 h (III).

Fig. 1 shows the FESEM and TEM images of the pre-formed VO₂ solid microspheres by the solvothermal method using isopropanol as the solvent. The FESEM image (Fig. 1a) demonstrates the solid VO₂ microspheres have a mean diameter of 1 μm and possess a uniform spherical morphology. As shown in Fig. 1b, the surface of the VO₂ solid microspheres consists of small nanoplates with thicknesses of approximately 20 nm. The TEM images (Fig. 1c and d) reveal the solid interior and the small plates on the surface of the VO₂ microspheres.

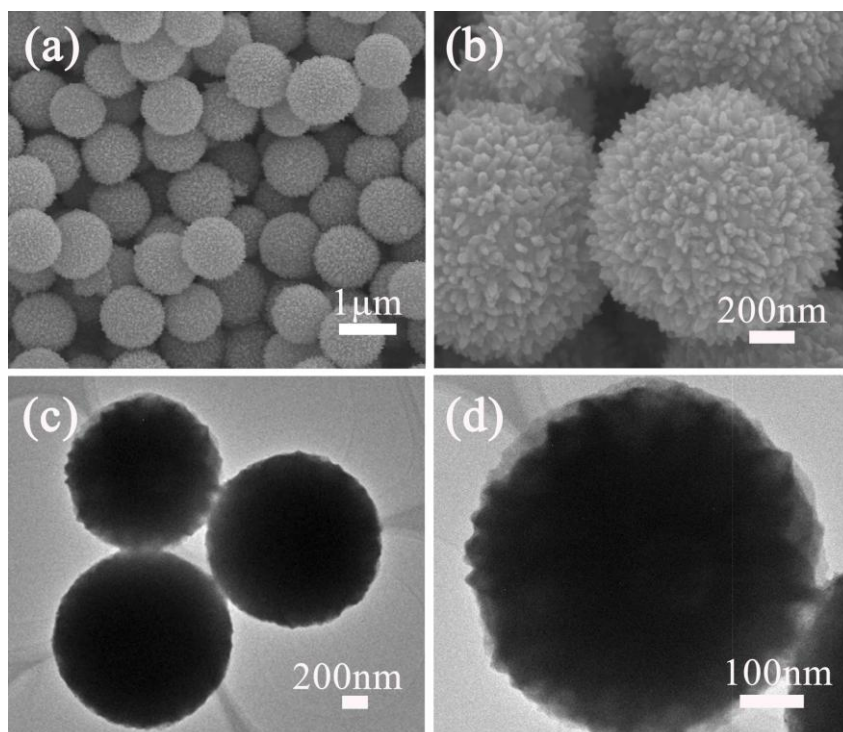


Figure 1. FESEM images (a, b) and TEM images (c, d) of the VO₂ microspheres synthesized at 200 $^{\circ}\text{C}$ after the solvothermal reaction for 2 h.

Fig. 2 shows the structural characterization results of the VO₂ microspheres after the solvothermal treatment in EG solvent for 36 h. The XRD pattern (Fig. 2a) of the solvothermal product is in good accordance with the standard peak positions of the monoclinic VO₂ phase, with lattice parameters of $a = 4.5968 \text{ \AA}$, $b = 5.6844 \text{ \AA}$, $c = 4.9133 \text{ \AA}$, and $\beta = 89.39^{\circ}$. This result demonstrates that the second solvothermal process did not change the phase of the VO₂ solid microspheres. Fig. 2b

shows the FESEM image of the VO₂-36 h solvothermal product, which has a uniform spherical morphology with a mean diameter of 1 μm. The TEM images (Fig. 2c and d) reveal the interior structure of the VO₂ microspheres, displaying the hollow interiors and the porous structure of the exterior shell. The results demonstrate the possibility of adjusting the interior structures of the VO₂ solid microspheres in different solvothermal solvents.

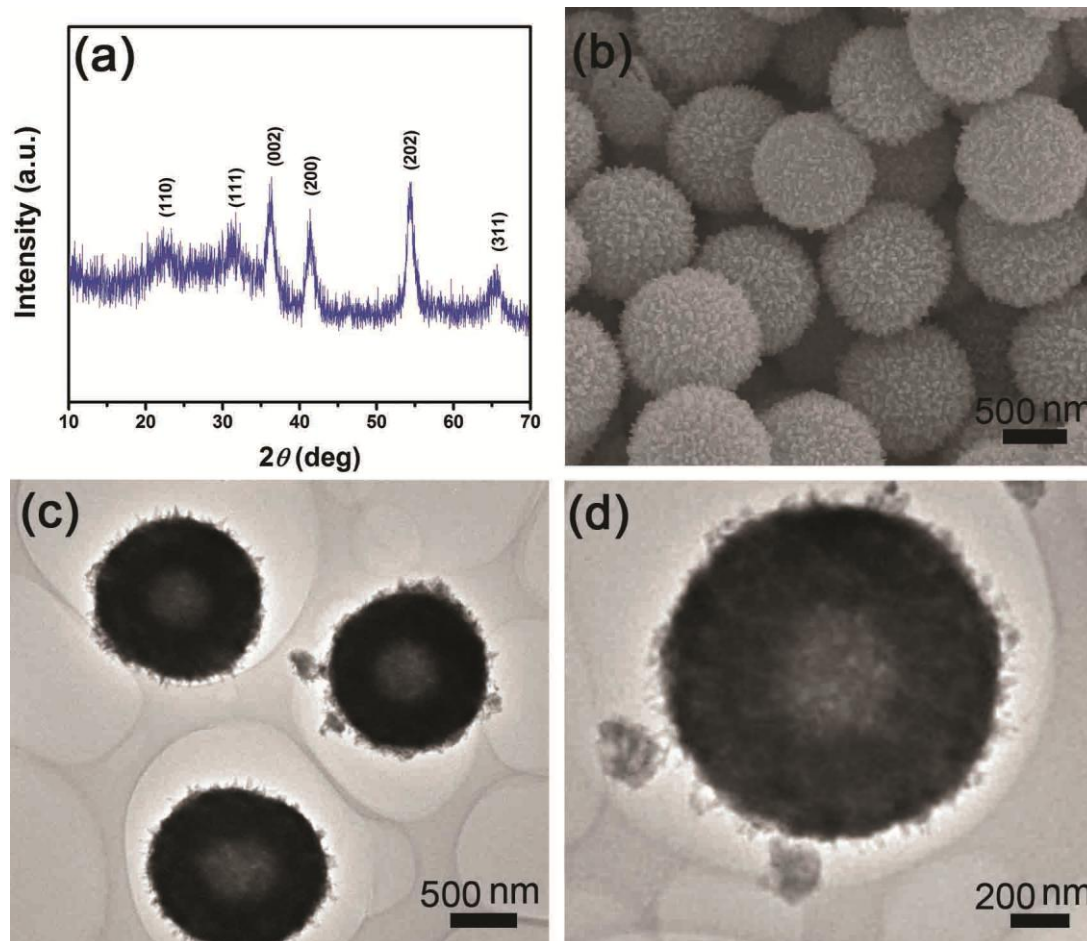


Figure 2. (a) XRD pattern, (b) FESEM image, and (c, d) TEM images of the VO₂-36 h hollow microspheres prepared via the two-step solvothermal process.

Time-dependent solvothermal experiments were carried out to study the structural evolution of the VO₂ solid microspheres into complete hollow microspheres. Fig. 3 shows the TEM images of the solvothermal products obtained by the solvothermal treatment of the VO₂ solid microspheres in EG solvent for 12 h, 24 h and 36 h. Fig 3a and b show the TEM images of the solvothermal products in EG solution after 12 h. A uniform yolk-shell structured interior was reliably fabricated, and a gap of 250 nm between the core and the shell was clearly seen. When the solvothermal time was extended to 24 h, double-shell structured VO₂ microspheres were obtained (Fig. 3c and d). The interior structures were converted into complete hollow structures after 36 h (Fig. 3e and f). The results indicate the structures of the solid microspheres changed from solid microspheres to yolk-shell, double-shell and then to

complete hollow microspheres. These structural evolutions can be explained by the inside-out Ostwald-ripening process, which generates the exterior crystalline shell via a depletion of the inner material[27, 28]. However, the Ostwald-ripening process ultimately leads to a completely hollow structure with a single shell[29, 30]. The dissolution of VO_2 at a specific area is attributed to its lower crystallinity and stability[31, 32]. When the solid microspheres are solvothermally treated sufficiently, the interior structures are dissolved to generate the completely hollow VO_2 microspheres.

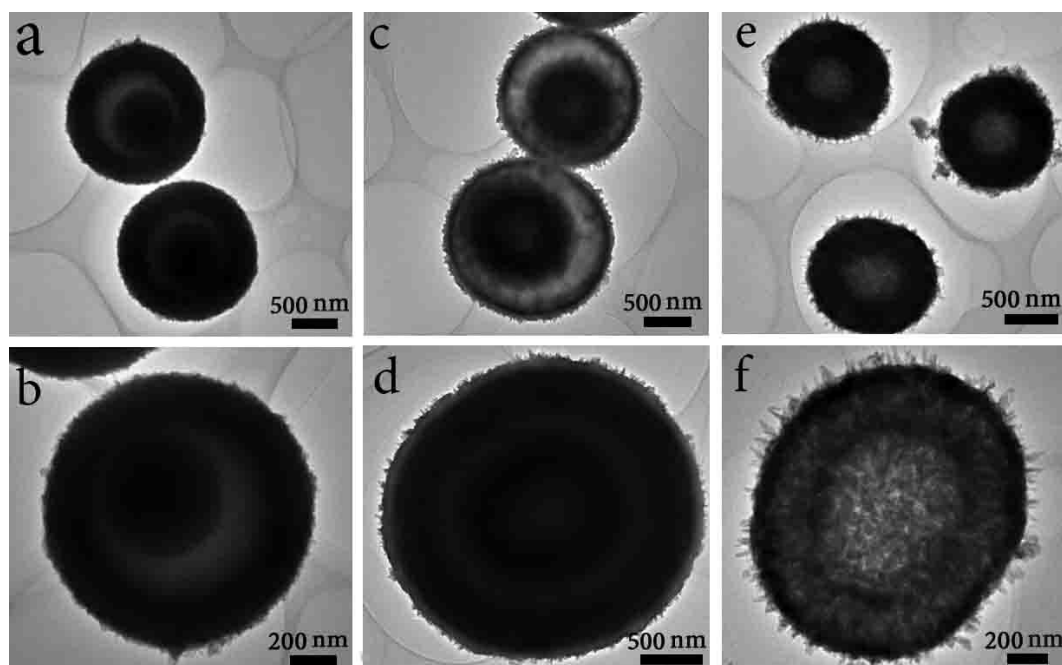


Figure 3. TEM images of the VO_2 microspheres obtained at different times of the second step solvothermal process: (a, b) 12 h, (c, d) 24 h, and (e, f) 36 h.

Fig. 4 shows the structural characterization results of the VO_2 -36 h hollow microspheres after annealing in air at $350\text{ }^\circ\text{C}$ for 2 h. The XRD pattern (Fig. 4a) indicates that VO_2 was completely transformed into V_2O_5 . The XRD peaks for the as-synthesized products are well indexed and assigned to the orthogonal structure of the V_2O_5 phase with a $Pmnm$ (56) space group (JCPDS card no. 41-1426, $a = 11.516\text{ \AA}$, $b = 3.566\text{ \AA}$, $c = 3.777\text{ \AA}$)[33]. As shown in Fig. 4b, the obtained V_2O_5 is composed of uniform microspheres with similar sizes as the VO_2 solid microspheres (Fig. 2b). The TEM images (Fig. 4c and d) demonstrate the homogenous hollow interior of the microspheres. The results suggest that the V_2O_5 hollow microspheres possess good structural preservation from the solvothermally prepared VO_2 -36 h hollow microspheres.

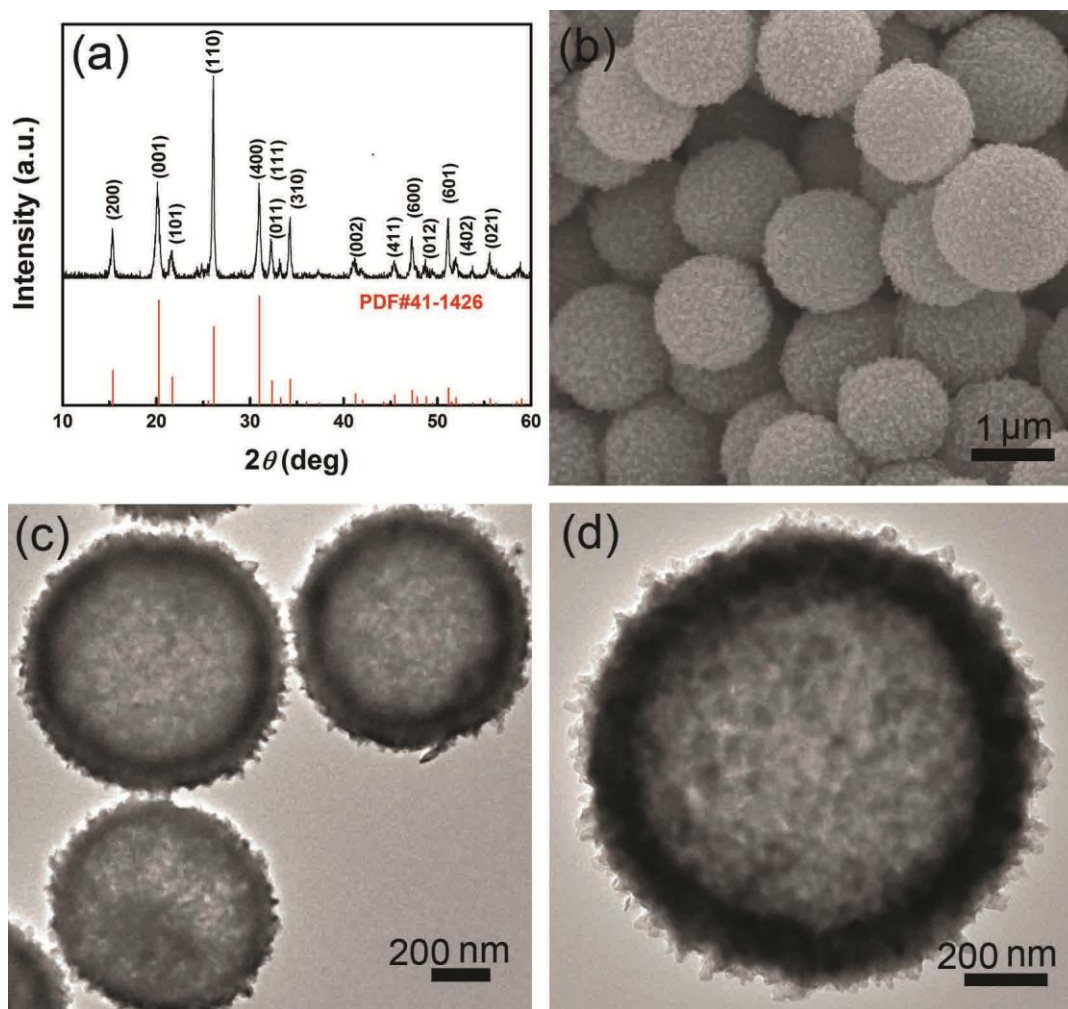


Figure 4. (a) XRD pattern, (b) FESEM image and (c, d) TEM images of the V_2O_5 hollow microspheres.

3.2 Electrochemical performance

The as-prepared V_2O_5 hollow microspheres were assembled into coin cells to evaluate their electrochemical performances, and the results are shown in Fig. 5. Fig. 5a shows the initial five successive CV curves of the V_2O_5 hollow microspheres in the voltage range of 2.5–4 V vs. Li/Li^+ at a scan rate of 0.1 mV s^{-1} . The two main peaks at 3.36 and 3.12 V during the cathodic scan indicate a multi-step lithium-ion intercalation process and the phase changes from $\alpha\text{-}V_2O_5$ to $\epsilon\text{-}Li_{0.5}V_2O_5$ (3.36 V) and then to $\delta\text{-}LiV_2O_5$ (3.12 V)[34]. The two peaks at 3.26 and 3.45 V in the following anodic scan are attributed to the lithium deintercalation process and the phase changes from $\delta\text{-}LiV_2O_5$ to $\epsilon\text{-}Li_{0.5}V_2O_5$ and then to $\alpha\text{-}V_2O_5$, respectively[35]. The shapes of the five CV curves are similar, suggesting good reversibility and cycling stability. Fig. 5b depicts the discharge and charge profiles of the 2nd, 10th, 20th, 30th, 50th, and 100th cycles for the V_2O_5 hollow microspheres at a current density of 100 mA g^{-1} . The discharge and charge plateaus are in good agreement with the peak positions in the CV curves (Fig. 4a). The two discharge plateaus at approximately 3.36 and 3.12 V are attributed to the phase transformations from $\alpha\text{-}V_2O_5$ to $\epsilon\text{-}Li_{0.5}V_2O_5$ and then to $\delta\text{-}LiV_2O_5$, respectively.

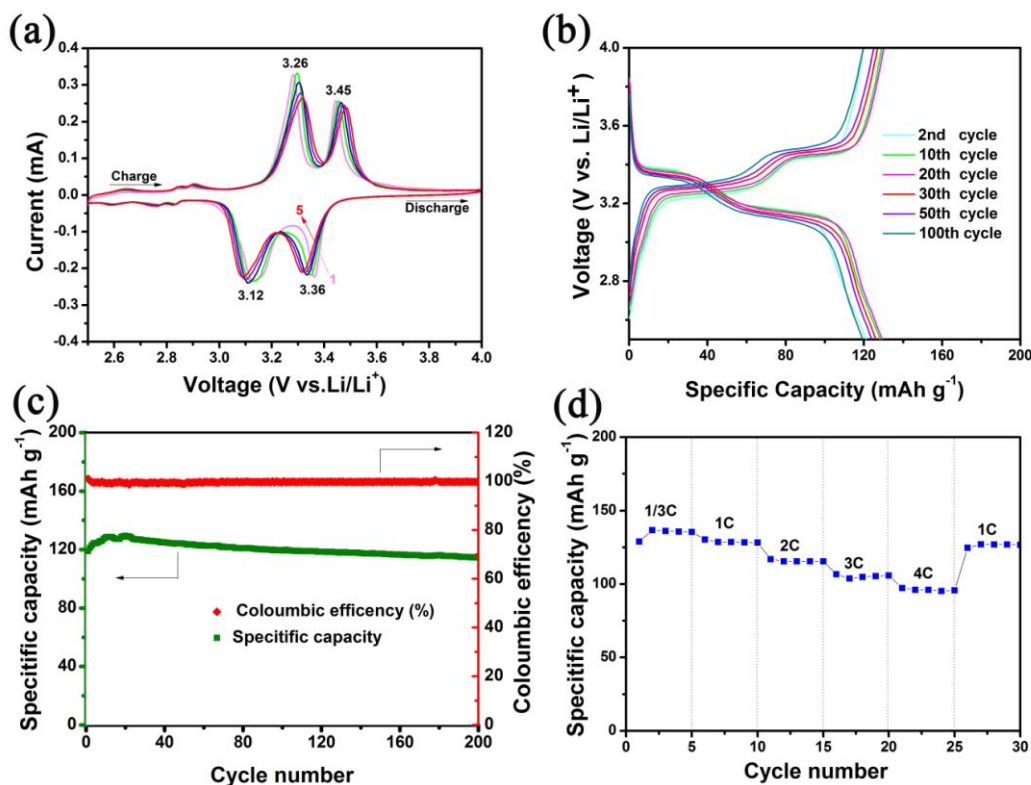


Figure 5. (a) CV curves of the V_2O_5 hollow microspheres at a scan rate of 0.1 mV s^{-1} in the voltage range between 2.5 V and 4 V vs. Li/Li^+ . (b) Galvanostatic discharge/charge profiles of selected cycles at a current density of 100 mA g^{-1} . (c) Cycling performance and coulombic efficiency of the V_2O_5 hollow microspheres. (d) Rate performance of the V_2O_5 hollow microspheres.

The discharge/charge curves of these cycles have similar plateaus, which again confirm that the electrode material has good electrochemical reversibility and cycle stability. Fig. 5c plots the cycling performance and coulombic efficiency of the hollow V_2O_5 microspheres at a current density of 100 mA g^{-1} . The V_2O_5 hollow microsphere electrode manifests a small capacity increase over the first twenty cycles, which is ascribed to the improved wettability of the electrode material and the activation of the electrode material by the initial electrochemical grinding process. An initial specific discharge capacity of 119 mA h g^{-1} was obtained for the V_2O_5 hollow microspheres. The capacity slowly increases to $129.4 \text{ mA h g}^{-1}$ at the 20th cycle. After 200 cycles, the hollow-structured V_2O_5 microspheres retain a capacity of $114.5 \text{ mA h g}^{-1}$. The average capacity fading rate is 0.07% per cycle, and the coulombic efficiency is near 100% . Fig. 5d shows the rate performance of the V_2O_5 hollow microspheres. A specific discharge capacity of 124 mA h g^{-1} at $1/3 \text{ C}$ was obtained for the V_2O_5 hollow microspheres, which reduces to 116 , 113 , 106 and 99 mA h g^{-1} at 1 C , 2 C , 3 C and 4 C ($1 \text{ C} = 147 \text{ mA h g}^{-1}$), respectively. When the current density is reset to 1 C , it retains a specific discharge capacity of 115 mA h g^{-1} . The results suggest that the electrode material has a good rate capability and reversibility. The as-synthesized V_2O_5 hollow microspheres demonstrate better cycling performance and rate capability when compared to other reported V_2O_5 microspheres and V_2O_5 flowers [36-37]. The previously reported vanadium oxide microspheres [36] showed good capacity retention, but only 50

cycles were reported. In addition, the other reported 3D hierarchical V₂O₅ flowers[37] also suffered from low capacity and rate capability. The superior rate performance reported here is attributed to the hollow structure of the microspheres. The hollow interiors of the microspheres can better accommodate volume changes upon repeated cycling, ensuring good structural integrity. Moreover, the contact area between the electrode and electrolyte can be enlarged, which can facilitate a good rate capability.

4. CONCLUSION

In summary, VO₂ microspheres with different interior structures were prepared from solid microspheres utilizing an additional solvothermal solution under the driving mechanism of Ostwald ripening. The obtained VO₂ microspheres were converted into V₂O₅ hollow microspheres with good structural preservation after annealing in air. As a cathode material for lithium-ion batteries, the hollow-structured V₂O₅ microspheres showed good cycling stability and rate capability. The preparation strategy may be applied for the synthesis of other materials.

ACKNOWLEDGEMENT

This work was supported by the National Natural Science Foundation of China (No. 51302323), the Program for New Century Excellent Talents in University (NCET-13-0594), Innovation-driven Project of Central South University (No.502501001) and the Research Fund for the Doctoral Program of Higher Education of China (No. 20130162120005).

References

1. Y.-Z. Zheng, H. Ding, E. Uchaker, X. Tao, J.-F. Chen, Q. Zhang, G. Cao, *J. Mater. Chem. A*, (2014) 1979.
2. Q. Yue, H. Jiang, Y. Hu, G. Jia, C. Li, *Chem. Comm.* 50 (2014) 13362.
3. M.L. Qin, J. Liu, S.Q. Liang, Q. Zhang, X.L. Li, Y. Liu, M.Y. Lin, *J. Solid State Electrochem.* 18 (2014) 2841.
4. J. Shao, X. Li, Z. Wan, L. Zhang, Y. Ding, L. Zhang, Q. Qu, H. Zheng, *ACS Appl. Mater. Interfaces*, (2013) 7671.
5. S. Wang, Z. Lu, D. Wang, C. Li, C. Chen, Y. Yin, *J. Mater. Chem.* 21 (2011) 6365.
6. X. Rui, J. Zhu, D. Sim, C. Xu, Y. Zeng, H.H. Hng, T.M. Lim, Q. Yan, *Nanoscale*, (2011) 4752.
7. S. Liang, X. Cao, Y. Wang, Y. Hu, A. Pan, G. Cao, *Nano Energy*, 22 (2016) 48.
8. M.S. Islam, C.A. Fisher, *Chem. Soc. Rev.* 43 (2014) 185.
9. Y.W. Lei Yao, J.H. Wu, M.W. Xiang, J.L. Li, B.Y. Wang, Y. Zhang, H.L. Hao Wu, *Inter. J. Electrochem. Sci.* 12 (2017) 206.
10. W. Lu, *Int. J. Electrochem. Sci.* (2017) 1118.
11. S. Liang, Y. Hu, Z. Nie, H. Huang, T. Chen, A. Pan, G. Cao, *Nano Energy*, 13 (2015) 58.
12. Y. Su, A. Pan, Y. Wang, J. Huang, Z. Nie, X. An, S. Liang, *J. Power Sources*, 295 (2015) 254.
13. S. Wang, S. Li, Y. Sun, X. Feng, C. Chen, *Energy Environ Sci.* 4 (2011) 2854.
14. X. Zhou, G. Wu, J. Wu, H. Yang, J. Wang, G. Gao, *Phys. Chem. Chem. Phys.* 16 (2014) 3973.
15. S.Q. Liang, M.L. Qin, Y. Tang, Q. Zhang, X.L. Li, X.P. Tan, A.Q. Pan, *Met. Mater. Int.* 20 (2014) 983.

16. A.Q. Pan, H.B. Wu, L. Zhang, X.W. Lou, *Energy Environ. Sci.* 6 (2013) 1476.
17. Y.N. Ko, Y. Chan Kang, S.B. Park, *Nanoscale*, 5 (2013) 8899.
18. J. Cheng, B. Wang, H.L. Xin, G. Yang, H. Cai, F. Nie, H. Huang, *J. Mater. Chem. A*, 1 (2013) 10814.
19. Y. Wang, K. Takahashi, K.H. Lee, G.Z. Cao, *Adv. Funct. Mater.* 16 (2006) 1133.
20. Y. Zhang, A. Pan, Y. Wang, W. Wei, Y. Su, J. Hu, G. Cao, S. Liang, *ACS Appl. Mater. Interfaces*, 8 (2016) 17303.
21. H.E. Wang, D.S. Chen, Y. Cai, R.L. Zhang, J.M. Xu, Z. Deng, X.F. Zheng, Y. Li, I. Bello, B.L. Su, *J. Colloid Interf. Sci.* 418 (2014) 74.
22. H.B. Wu, A.Q. Pan, H.H. Hng, X.W. Lou, *Adv. Funct. Mater.* 23 (2013) 5669.
23. A. Pan, T. Zhu, H.B. Wu, X.W. Lou, *Chem. Eur. J.* 19 (2013) 494.
24. E. Uchaker, N. Zhou, Y. Li, G. Cao, *J. Phys. Chem. C*, 117 (2013) 1621.
25. A. Pan, H.B. Wu, L. Yu, X.W. Lou, *Angew. Chem. Int. Ed.* 52 (2013) 2226.
26. L. Zeng, A. Pan, S. Liang, J. Wang, G. Cao, *Sci. China Mater.* 59 (2016) 567.
27. X.W. Lou, L.A. Archer, Z. Yang, *Adv. Mater.* 20 (2008) 3987.
28. Y. Zhao, L. Jiang, *Adv. Mater.* 21 (2009) 3621.
29. X.B. Cao, L. Gu, L.J. Zhuge, W.J. Gao, W.C. Wang, S.F. Wu, *Adv. Funct. Mater.* 16 (2006) 896.
30. J.G. Yu, H. Guo, S.A. Davis, S. Mann, *Adv. Funct. Mater.* 16 (2006) 2035.
31. P.W. Voorhees, *J. Stat. Phys.* 38 (1985) 231.
32. H. G. Yang, H. C. Zeng, *J. Phys. Chem. B*, 108 (2004) 3492.
33. A.-M. Cao, J.-S. Hu, H.-P. Liang, L.-J. Wan, *Angew. Chem. Int. Ed.* 44 (2005) 4391.
34. Y.-S. Hu, X. Liu, J.-O. Müller, R. Schlögl, J. Maier, D.S. Su, *Angew. Chem. Int. Ed.* 121 (2009) 216.
35. A. Odani, V.G. Pol, S.V. Pol, M. Koltypin, A. Gedanken, D. Aurbach, *Adv. Mater.* 18 (2006) 1431.
36. H. Fei, W. Feng, Y. Lin, *Solid State Sci.* 55 (2016) 36.
37. H. Pang, Q. Song, P. Tian, J. Cheng, N. Zou, G. Ning, *Mater. Lett.* 171 (2016) 5.

© 2017 The Authors. Published by ESG (www.electrochemsci.org). This article is an open access article distributed under the terms and conditions of the Creative Commons Attribution license (<http://creativecommons.org/licenses/by/4.0/>).